A Multimode/Multiband Envelope Tracking Transmitter With Broadband Saturated Amplifier

Junghwan Moon, *Student Member, IEEE*, Junghwan Son, Juyeon Lee, and Bumman Kim, *Fellow, IEEE*

***Abstract*—A multimode/multiband envelope tracking (ET) transmitter consisting of a hybrid switching amplifier (HSA) and a broadband saturated power amplifier (PA) is developed for operation across 1.3 to 2.7 GHz. For the various standard signals with different bandwidth (BW) and peak-to-average power ratio, the HSA efficiently provides supply signals to the PA by changing the reference value of the hysteresis comparator. The saturated amplifier employs the nonlinear output capacitor to shape the voltage waveform, resulting in the half-sinusoidal or rectangular waveform. Since the nonlinear capacitor generates large out-of-phased second harmonic component with small higher order harmonics, the voltage shaping is mainly carried out by the capacitor and slightly supported by the harmonic loading circuit. Thus, with the harmonic load higher than that of output capacitor, the saturated amplifier can operate with high efficiency. This characteristic enables the saturated PA to operate with broadband characteristic and high efficiency because the design is mainly focused on the fundamental matching problem while the harmonics can be easily kept out of a low efficiency region through the subsequent optimization of the matching circuit. The broadband saturated PA is implemented based on load/source-pull methodology. The broadband matching networks for the high efficiency are synthesized using the simplified real frequency technique. For the BW from 1.3 to 2.7 GHz (70% fractional BW), the measured output power, drain efficiency, and power-added efficiency (PAE) performances are between 39.8–42.0 dBm, 55.8–69.7%, and 51.2–65.3%, respectively. The multimode/multiband ET transmitter with the designed broadband saturated PA is demonstrated at 1.8425-GHz long-term evolution (LTE), 2.14-GHz wideband code division multiple access (WCDMA), and 2.6-GHz mobile world wide interoperability for microwave access (m-WiMAX) applications. This transmitter delivers a PAE of 32.16, 37.24, and 28.75% for LTE, WCDMA, and m-WiMAX applications.**

***Index Terms*—Broadband power amplifier (PA), efficiency, envelope tracking, multiband, multimode, nonlinear capacitor, saturated PA.**

I. Introduction

As WIRELESS communication systems evolve, mobile equipment should be able to handle text, voice, multimedia, and broadcast information with global roaming capability. In addition, independently developed standards, such as long-term evolution (LTE), mobile world wide interoperability for microwave access (m-WiMAX), and wideband code division multiple access (WCDMA), increase the number of frequency bands and spectrum fragmentation. Therefore, power amplifiers (PAs) for the systems should have multimode and multiband capability to cover a number of functions. Moreover, to efficiently use limited frequency resources, signals of the communication systems are coded by a complex modulation method, increasing the signal bandwidth (BW) and peak-to-average power ratio (PAPR). Such large PAPR signals push the PA operation into a large back-off power region to satisfy the stringent linearity requirements of the systems, decreasing amplification efficiency. Therefore, to improve efficiency at the back-off power levels, many efficiency enhancement techniques have received a lot of attention for the last few decades [1]–[19].

The Doherty PA and envelope tracking (ET) transmitter have been extensively investigated to increase the efficiency at the low power region. The Doherty amplifier modulates the load impedance of the main cell according to the power level by using a quarter-wave impedance transformer [3]–[9]. However, this transformer is sensitive to the frequency, preventing the broadband operation. On the other hand, the ET transmitter modulates the supply voltage of the PA in the transmitter to push the PA in the saturated region, thus delivering the maximum efficiency regardless of the power level [10]–[14]. The transmitter consists of the supply modulator and the PA. The modulator is capable of handling the multimode signal with high efficiency. Also, it is not related to the operating frequency band [12]. However, the PA is sensitive to the frequency and should have the broadband capability with high efficiency. Therefore, for the multimode and multiband operation, the ET transmitter is superior to the Doherty amplifier.

In general, high efficiency PAs employ multiple resonators to manipulate the current and voltage waveforms for reducing power dissipation in the transistor. However, these resonators are very sensitive to the frequency, thus leading to narrow band characteristic. In [15], the broadband class-J PA has been introduced. Even though the class-J amplifier does not employ any harmonic-short circuits, a proper second harmonic load is required to maintain the half-sinusoidal voltage and current waveforms across the broad bandwidth. Recently, the harmonic load/source-pull techniques are extensively studied to deliver high efficiency across a wide BW [16]–[18]. These designs have one thing in common. That is, for high efficiency across the broad BW, the fundamental load impedance should be properly matched and the harmonic load impedances have a large tolerance. However, there is no physical explanation for these designs.

Manuscript received June 19, 2011; revised September 20, 2011; accepted September 23, 2011. Date of publication November 04, 2011; date of current version December 14, 2011. This work was supported by The Ministry of Knowledge Economy (MKE), Korea, under the Information Technology Research Center (ITRC) support program supervised by the National IT Industry Promotion Agency (NIPA) (NIPA-2011-(C1090-1111-0011)), by World Class University (WCU) program funded by the Ministry of Education, Science and Technology through the National Research Foundation of Korea (R31-10100), and by the Brain Korea 21 Project in 2011. This paper is an expanded paper from the IEEE International Microwave Symposium, Baltimore, MD, June5–10, 2011.

The authors are with the Department of Electrical Engineering and Division of Information Technology Convergence Engineering, Pohang University of Science and Technology, Pohang, Gyeongbuk 790-784, Korea (e-mail: jhmoon@postech.ac.kr; jhson@postech.ac.kr; davinch@postech.ac.kr; bmkim@postech.ac.kr).

Digital Object Identifier 10.1109/TMTT.2011.2170580

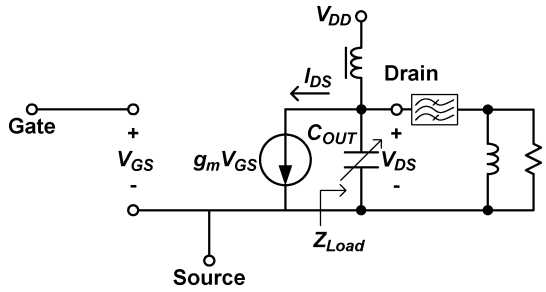

Fig. 1. Simplified block diagram of the saturated amplifier.

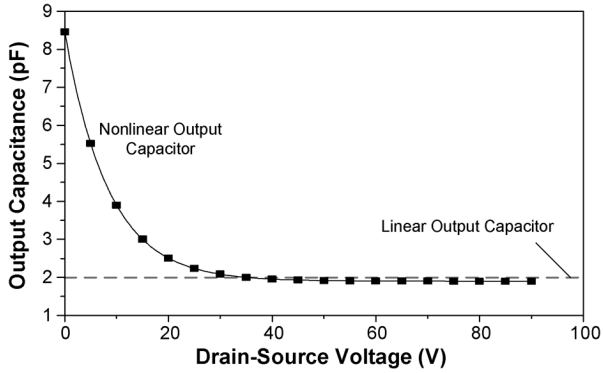

Fig. 2. Nonlinear behavior of the output capacitor. This capacitor includes the nonlinear $C_{\rm ds}$ and $C_{\rm gd}$.

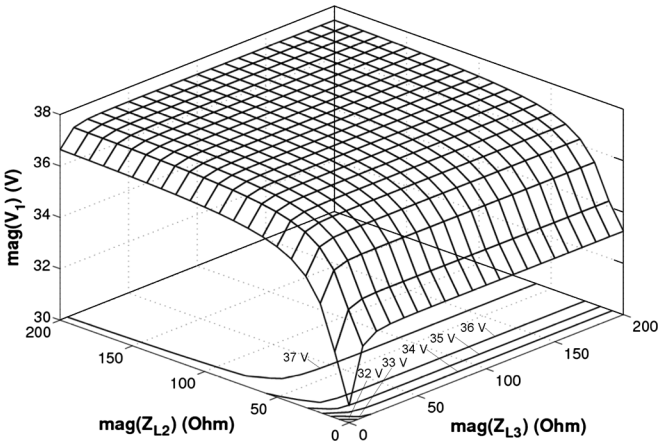

Fig. 3. Magnitude of the fundamental voltage component across the nonlinear capacitor according to the harmonic load impedances. During the simulation, the fundamental load impedance is tuned to achieve the maximum voltage swing.

In this paper, we design a multimode/multiband ET transmitter with a broadband saturated amplifier for femto-cell applications. Though the multimode/multiband ET PA is demonstrated in [19], this paper presents more detailed analyses for the broadband saturated amplifier and experimental results. For the various standards with different signal BWs and PAPRs, the supply modulator, configured by the hybrid switching amplifier (HSA), provides a supply voltage with high efficiency by adopting the proper reference value of the hysteresis comparator [12]. For high efficiency and broadband PA, the saturated amplifier is employed [20]–[22]. This amplifier takes advantage of the nonlinear output capacitor $C_{\rm out}$, consisting of the nonlinear drain-to-source capacitance $C_{\rm ds}$ and gate-to-drain capacitance $C_{\rm gd}$, to shape the voltage waveform. For the external harmonic loads larger than $C_{\rm out}$, the waveform shaping is mainly carried out by the harmonic components generated by the $C_{\rm out}$. Thus, without any elaborated harmonic control circuitries, this amplifier can deliver high efficiency across a wide BW. The wideband source and load impedances are found using the load/source-pull methodology, then synthesized using the simplified real frequency technique (SRFT) across 1.3 to 2.7 GHz [23], [24]. The multimode/multiband ET transmitter is demonstrated for 1.8425-GHz LTE, 2.14-GHz WCDMA, and 2.6-GHz m-WiMAX applications.

II. Broadband Saturated Power Amplifier

A. Saturated Power Amplifier

The simplified block diagram of the saturated amplifier proposed in [20]–[22] is depicted in Fig. 1. In general, the high efficiency PAs employ a special harmonic circuitry, which is open or short circuit for the particular harmonic frequency, to achieve a specific voltage waveform such as half-sinusoidal or rectangular shape. On the other hand, the saturated amplifier creates the required voltage waveform using the harmonic component generated by the nonlinear output capacitor, as described in Fig. 2. If the external harmonic load impedances are larger than $C_{\rm out}$, the waveform shaping can be accomplished. Since the harmonic voltage generated by $C_{\rm out}$ is mostly the second harmonic component with a small third harmonic, the resulting voltage waveform is half-sinusoidal, increasing the fundamental voltage component. Sometimes, the rectangular shape may appear depending on the external harmonic load, which will be shown in Section II-B. Due to the saturated operation, the current waveform of the PA is bifurcated. Thus, the waveforms of the amplifier are the same as those of the class-$\rm F^{-1}$, but the harmonic circuit topology is similar to the class-E amplifier with a tuned fundamental load. The fundamental load should be between $\sqrt{2}R_{\rm opt}$ to $2R_{\rm opt}$ because of the enlarged fundamental voltage and reduced fundamental current components [21]. To explore the harmonic generation property and voltage shaping of the nonlinear $C_{\rm out}$, the simulation is carried out using the circuit diagram in Fig. 1. During the simulation, it is assumed that a purely sinusoidal input signal is excited, generating only the fundamental current at the dependent current source. The fundamental load impedance is matched to deliver the maximum voltage swing, generating high efficiency and output power. Fig. 3 shows the magnitude of the fundamental voltage component across the nonlinear $C_{\rm out}$ according to the magnitude of external harmonic load impedances. For the loads two or three times larger than the impedance level of $C_{\rm out}$, a large fundamental voltage can be maintained. When all harmonics are shorted, the fundamental voltage is 30 V. In this simulation, the impedance levels of $C_{\rm out}$ at the fundamental, second, and third harmonic frequencies are $j30\ \Omega$, $j15\ \Omega$, and $j10\ \Omega$, respectively. Therefore, the highly efficient operation can be accomplished by the harmonic generation of the nonlinear capacitor if the fundamental load

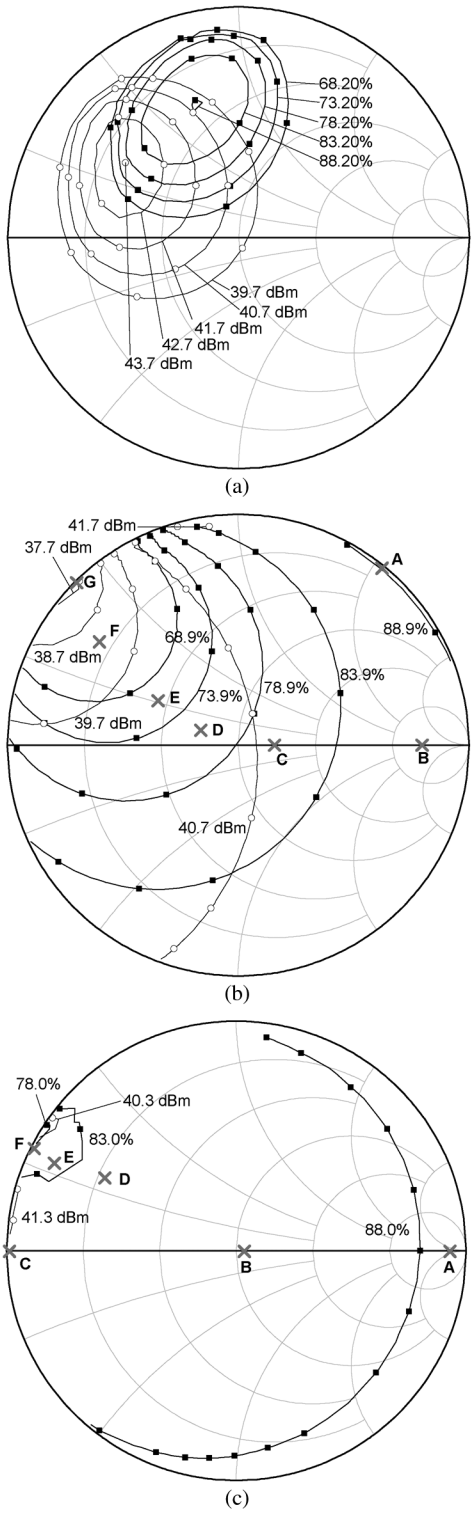

Fig. 4. Harmonic load-pull contours of Cree GaN HEMT CGH60015 bare-chip model: (a) fundamental (2.0 GHz), (b) second harmonic (4.0 GHz), and (c) third harmonic (6.0 GHz).

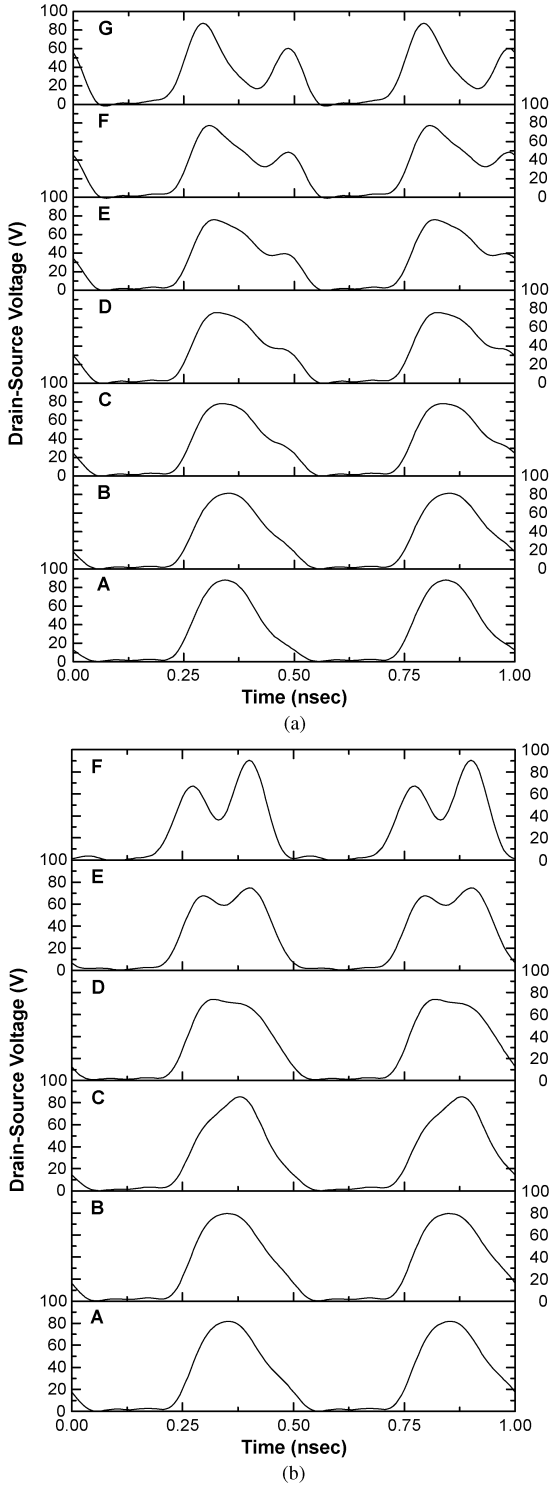

Fig. 5. (a) Voltage waveforms for the various second harmonic loads, located in Fig. 4(b), when the third harmonic load is set to 1000 Ω. (b) Voltage waveforms for the various third harmonic loads, located in Fig. 4(c), when the second harmonic load is set to 1000 Ω.

impedance is matched to the proper region and the harmonic loads are larger than $C_{\rm out}$.

B. Broadband Capability of Saturated Power Amplifier

In contrast to the conventional high efficiency PA, the voltage waveform shaping of the saturated amplifier is accomplished by the nonlinear output capacitor and the current waveform is shaped by the saturated operation. Those shapings are not sensitive to the harmonic loads, which makes it easy to design broadband PA, as explained in Section II-A. In order to demonstrate the large tolerance of the harmonic load for a real device, a harmonic load-pull simulation is carried out using Cree

GaN HEMT CGH60015 bare-chip large signal model at 2.0 GHz. In the simulation, other harmonics above the third harmonic at the load are set to 1000 Ω, leading that the higher harmonics are terminated by nonlinear $C_{\rm out}$. Moreover, all harmonics at the source are shorted, resulting in the pure sinusoidal voltage across the input capacitor of the device. Fig. 4 shows the harmonic load-pull simulation results. For a reference, the maximum efficiency of the PA with short circuit for all harmonics is 66.9%. As mentioned in Section II-A, the simulation results clearly show that the saturated amplifier delivers high efficiency for a broad range of harmonic loads, verifying the harmonic generation by the nonlinear capacitor. In addition, the resulting voltage waveforms according to the harmonic loads marked on Fig. 4(b) and (c) are depicted in Fig. 5. Although the nonlinear capacitor generates a lot of second harmonic with a few high-order voltage components, the voltage waveform could be either a half-sinusoidal or quasi-rectangular waveform depending on the harmonic load impedance. However, the maximum efficiency is obtained from the half-sinusoidal voltage waveform.

Above simulation is carried out under the assumption that the third harmonic or second harmonic is open circuit during the second or third harmonic load-pull simulation. To explore the large tolerance according to the harmonic impedance level, the second/third load-pull simulation is conducted for the fixed third/second harmonic loads. Fig. 6 and Fig. 7 show the second and third harmonic load-pull simulation results when the third harmonic and second harmonic are placed on 0.001, 10, 100, and 1000 Ω, respectively. In particular, Fig. 6(a) is the class-F^{-1} condition and Fig. 7(a) is the class-F condition. These figures show that a large tolerance is allowed when the fixed harmonic impedance is larger because the voltage waveform shaping of the amplifier is mostly accomplished by the nonlinear output capacitor. This result indicates that, for the broadband operation, only the fundamental load should be carefully matched to the impedance trajectory having high efficiency across the targeted BW, while the harmonic loads are kept high impedance region.

C. Design of Broadband Saturated Amplifier

Since the external harmonic load has a large tolerance for shaping the voltage waveform, a broadband operation with high efficiency can be realized easily by properly matching the fundamental load only. Broadband matching can be accomplished by adopting the multi-section matching network because the impedance transformation ratio of the network can be reduced, lowering the quality factor and maintaining nearly constant load impedance. The PA operates at a large signal level and the nonlinear intrinsic capacitor, which is varied with respect to the power level, should be considered. In addition, the commercial power transistors are in the package. Thus, the broadband PA design should be carried out at the package plane. The nonlinear elements in the power device and package effect make the design of the broadband matching network difficult. Thus, the design based on the harmonic load/source-pull methodology across the desired BW is preferred.

In this work, a broadband saturated PA is designed using Cree GaN HEMT CGH40010 device, consisting of CGH60015 bare-chip and package, with a goal of above 60% efficiency

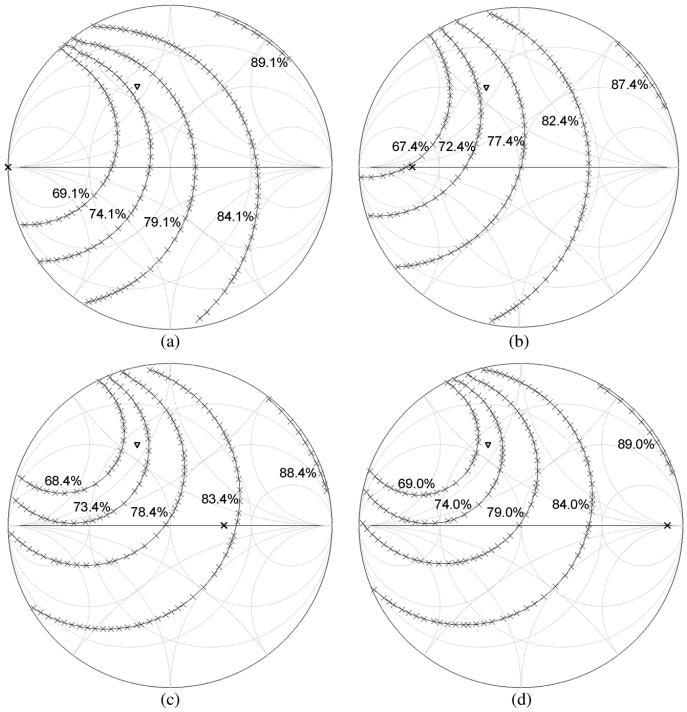

Fig. 6. Second harmonic load-pull contours for the various third harmonic loads, marked by × on the Smith chart, of (a) 0.001, (b) 10, (c) 100, and (d) 1000 Ω. During the simulations, the fundamental load impedance, marked by ▽, is set to $21 + j29.253\ \Omega$ for maximum efficiency.

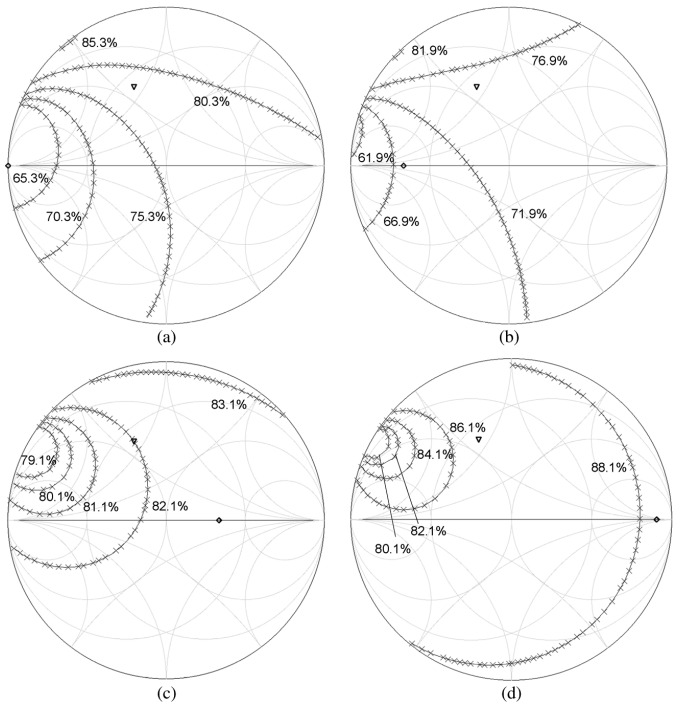

Fig. 7. Third harmonic load-pull contours for the various second harmonic loads, marked by ◇ on the Smith chart, of (a) 0.001, (b) 10, (c) 100, and (d) 1000 Ω. During the simulations, the fundamental load impedance, marked by ▽, is set to $21 + j29.253\ \Omega$ for maximum efficiency.

over the 70% fractional BW from 1.3 to 2.7 GHz. In the design and implementation, the device is biased at drain-source voltage $V_{\rm ds}$ of 30 V with idle current $I_{\rm dsq}$ of 200 mA. As mentioned above, the broadband design is carried out using the harmonic load/source-pull simulation. During the simulation, to

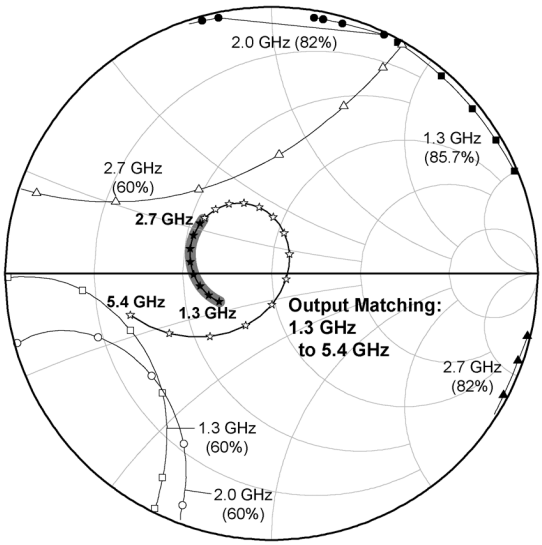

Fig. 8. Simulated second harmonic load-pull contour for the efficiencies of 60% at 1.3, 2.0, and 2.7 GHz.

guarantee the stability and flat gain response across the desired BW, the parallel RC network is attached at the transistor's gate-terminal, as shown in Fig. 10. In addition, the bias lines of the gate and drain are attached at the terminals. Thus, the broadband matching network is located outside of the circuit. Fig. 8 shows the simulated second harmonic load-pull contours for the efficiencies of 60% at 1.3, 2.0, and 2.7 GHz. Compared to the harmonic load-pull simulation result of the bare-chip model in Fig. 4, the tolerance of the harmonic load impedance is reduced because of the package effect. However, high efficiency still can be achieved for the broad region of the second harmonic load without requiring any additional design efforts. The second harmonic load is matched for high efficiency through the proper placement of the bias line and subsequent optimization of the fundamental matching network. Fig. 9 shows the simulated fundamental load/source-pull contours for the efficiencies of 60% at 1.3, 2.0, and 2.7 GHz. For the broadband operation with the targeted performance, the fundamental source and load impedances should be located within the required matching region. With the targeted fundamental load and source impedances across 1.3 to 2.7 GHz, the matching networks are designed by SRFT. In the synthesis, two-section low-pass LC networks are employed for the matching networks. The resultant impedances of the LC matching circuit generated by SRFT are overlaid by dark gray lines in Fig. 9, which is properly matched to the desired impedances. The calculated LC elements are converted into a distributed network, and the optimization algorithm is conducted to finely adjust the width and length of the transmission line for the fundamental matching. During the optimization, we also make an effort to be high impedance for the harmonic impedances. The resultant impedances of the transmission line matching networks are also overlaid by $(-\star-)$ in Fig. 9.

D. Implementation and Experimental Results

Using the designed matching networks in Section II-C, the broadband saturated amplifier is fabricated as shown in Fig. 10.

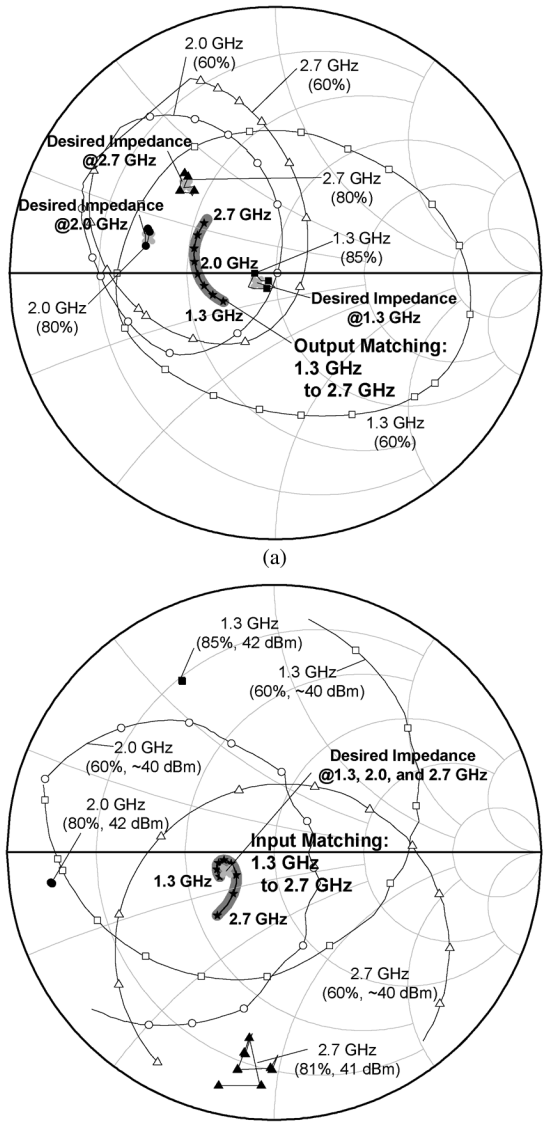

Fig. 9. Simulated fundamental (a) load-pull and (b) source-pull contours for the efficiencies of 60% at 1.3, 2.0, and 2.7 GHz.

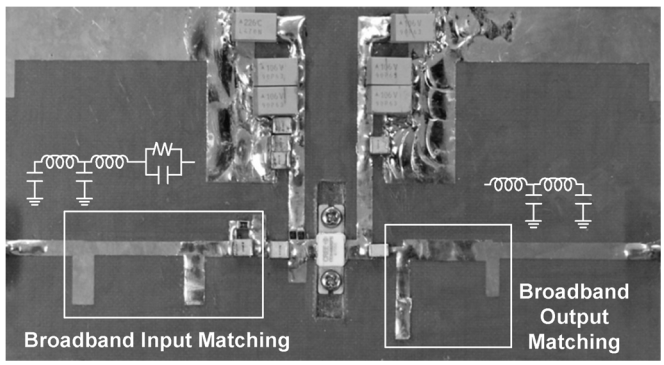

Fig. 10. Photo of the designed broadband saturated amplifier.

The amplifier is implemented on a Taconic TLY-5 substrate with $\varepsilon_r = 2.2$ and thickness of 31 mil. In the experiment, the amplifier is biased at $V_{\rm ds}$ of 30 V with $I_{\rm dsq}$ of 200 mA.

Fig. 11 shows the measured and simulated S-parameters of the implemented amplifier. A reasonable agreement between the simulation and implementation results can be noted up to 4

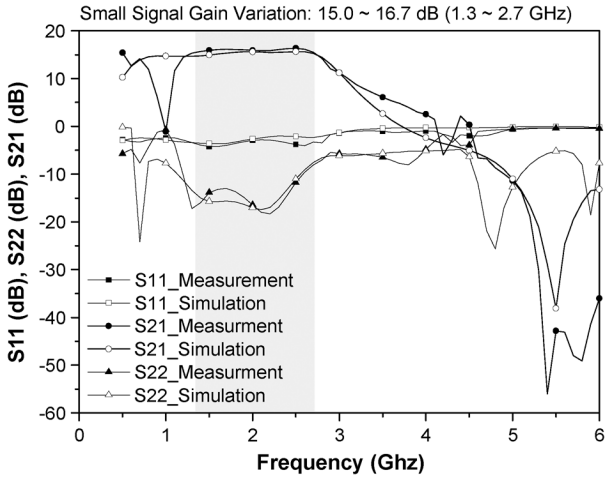

Fig. 11. Measured and simulated S-parameters of the designed amplifier.

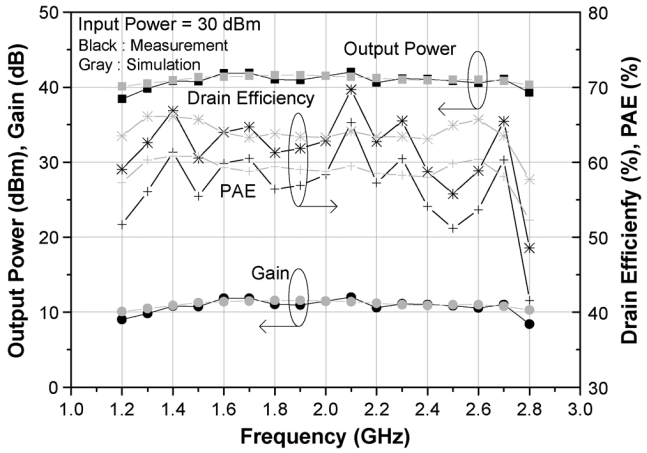

Fig. 12. Measured and simulated output power, gain, efficiency, and PAE of the implemented amplifier across the bandwidth from 1.2 to 2.8 GHz when the input power is 30 dBm.

TABLE I
STATE-OF-THE-ART BROADBAND PAS

Ref.	BW (GHz / %)	P_{out} (dBm)	Gain (dB)	DE (%)
[15]	1.40−2.60 / 60	39.0−40.0	10.2−12.2	60.0−70.0
[16]	1.90−2.90 / 42	45.0−47.0	10−12	60.0−65.0
[17]†	1.90−4.30 / 78	40.0−42.0	9−11	57.0−72.0
[18]	1.50−2.75 / 60	38.5−41.5	8−11	71.4−84.0
This Work	1.30−2.70 / 70	39.8−42.0	9.8−12.0	55.8−69.7

† The broadband PA is implemented using bare-chip.

GHz. For the targeted BW from 1.3 to 2.7 GHz, the small signal gain of the implemented amplifier is between 15.0–16.7 dB. The broadband amplifier is characterized using a constant input power of 30 dBm. As shown in Fig. 12, the measured and simulated output power, drain efficiency (DE), and PAE performances are between 39.8–42.0 dBm, 55.8–69.7%, and 51.2–65.3%, respectively, in the frequency range of 1.3 to 2.7 GHz. These performances are summarized in Table I together with those of the state-of-the-art broadband PAs.

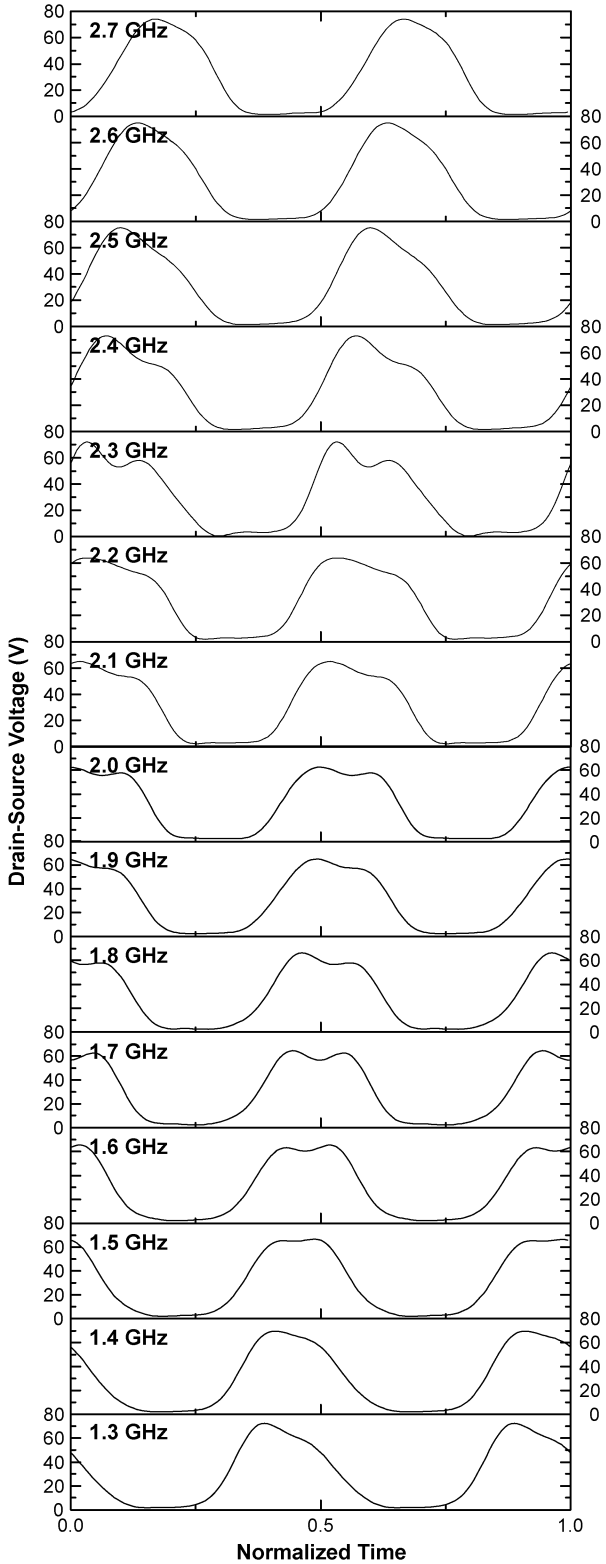

Fig. 13. Simulated drain-source voltage waveforms of the designed broadband amplifier over 1.3 to 2.7 GHz when the input power is 30 dBm.

Fig. 13 shows the simulated drain-source voltage waveforms of the designed broadband saturated amplifier over 1.3 to 2.7 GHz when the input power is 30 dBm. As mentioned in Section II-A, the half-sinusoidal or quasi-rectangular waveform appears depending on the harmonic load impedances. The

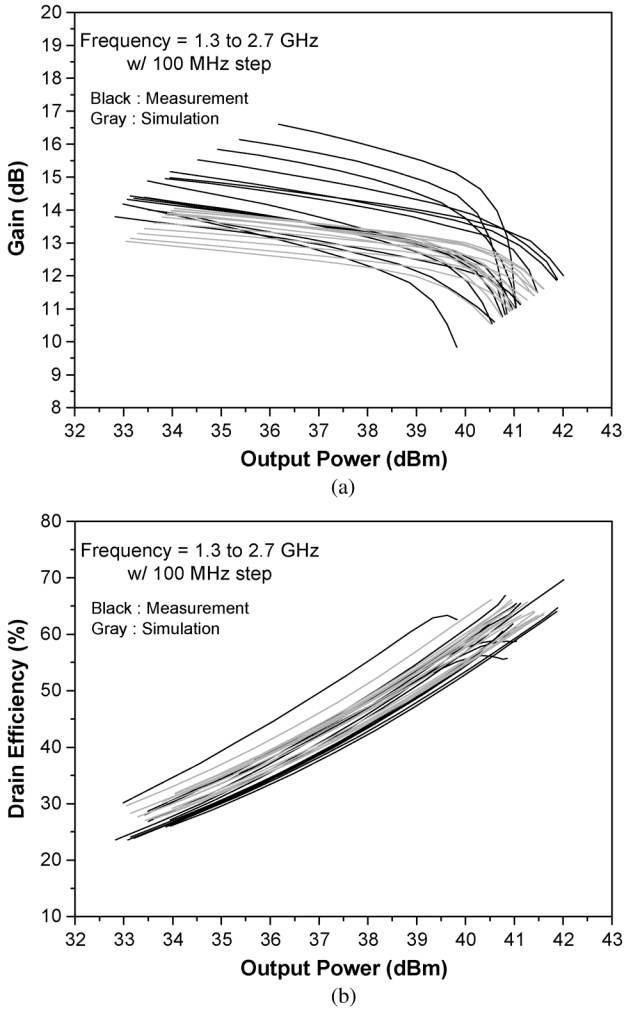

Fig. 14. Measured and simulated (a) gain and (b) efficiency of the implemented amplifier across 1.3 to 2.7 GHz with 100 MHz step.

efficiency is higher for the frequency band having the half-sinusoidal voltage waveform than the frequency band having the quasi-rectangular waveform because the half sinusoidal voltage waveform contains a fundamental voltage 1.4 times larger than the quasi-rectangular shape, when considering up to third harmonic. In Fig. 14, we compare the measured and simulated gain and DE over the targeted BW according to the output power.

The implemented amplifier is tested using modulated signals. A number of standards and frequency bands are located in the targeted bandwidth of 1.3 to 2.7 GHz. Among them, LTE, WCDMA, and m-WiMAX downlink signals are employed for demonstration. In particular, the amplifier is tested at 1.8425-GHz LTE (10-MHz BW and 6.5-dB PAPR), 2.14-GHz WCDMA (5-MHz BW and 7.0-dB PAPR), and 2.6-GHz m-WiMAX (10-MHz BW and 8.5-dB PAPR) signals. The same signals are also employed to demonstrate the multimode/multiband saturated ET transmitter, which will be described in Section III. Fig. 15 shows the measured efficiency and adjacent channel leakage ratio (ACLR) characteristics before and after linearization. The linearization is carried out using the commercial digital predistortion (DPD) board. The amplifier

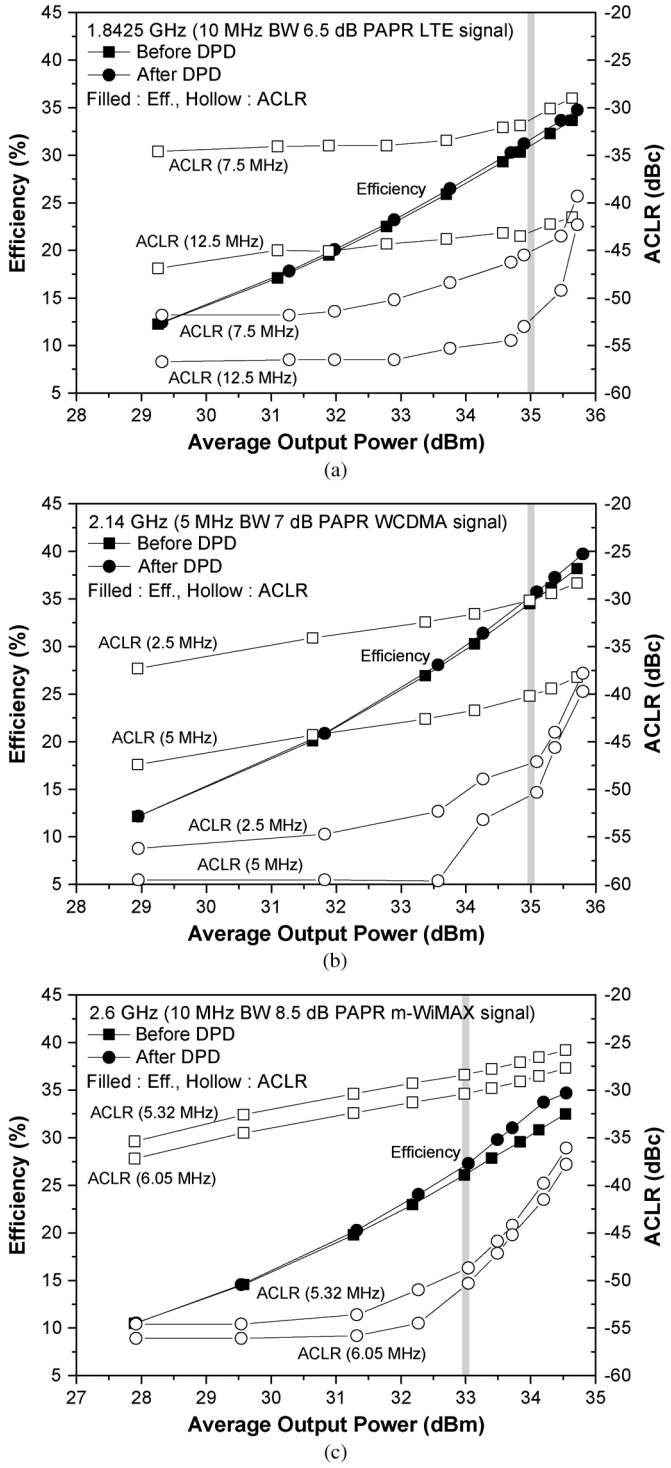

Fig. 15. Measured efficiency and ACLR characteristics before and after linearization at (a) 1.8425 GHz with LTE signal, (b) 2.14 GHz with WCDMA signal, and (c) 2.6 GHz with m-WiMAX signal.

delivers a quite linear characteristic with high efficiency. For the LTE signal, the amplifier delivers a DE of 31.2% at an average output power of 34.9 dBm. By adopting the linearization technique, the ACLR of the amplifier at the frequency offset of 7.5 MHz is −45.5 dBc, satisfying the linearity requirement of the LTE specification. For the WCDMA application, DE and ACLR at an average output power of 35.1 dBm are 35.8% and

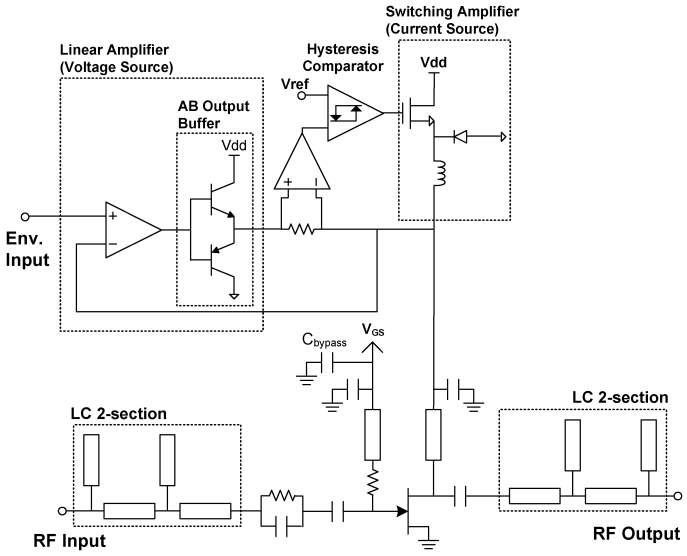

Fig. 16. Multimode/multiband ET transmitter with the broadband saturated amplifier.

−47.1 dBc, respectively, which are measured at the frequency offset of 2.5 MHz after the linearization. For the m-WiMAX signal, the amplifier delivers a DE of 29.8% at an average output power of 33.5 dBm. At the same average power, the ACLR of the linearized amplifier at the frequency offset of 5.32 MHz is −45.9 dBc. These results clearly show that the implemented broadband saturated amplifier is suitable to amplify modern communication signals for wide range of frequencies.

III. Multimode/Multiband ET Transmitter

To improve the efficiency of the implemented broadband saturated amplifier at the back-off power level while maintaining the broadband capability, $V_{\rm ds}$ of the amplifier is modulated according to the input signal level. Fig. 16 illustrates the multimode/multiband ET transmitter with the broadband saturated amplifier. This transmitter consists of the broadband saturated PA, implemented in Section II, and a supply modulator configured in HSA [12].

The HSA is composed of a linear amplifier and a switching amplifier. The linear amplifier works as an independent voltage source throughout the feedback network, while the switching amplifier operates as a dependent current source. By detecting the current polarity at the output of the linear amplifier, the state of the switching amplifier is changed through the hysteresis comparator. Thus, most of the current required for the PA is supplied by the efficient switching amplifier, and additional current is provided by the linear amplifier. Since the residual current from the switching amplifier is sinked by the linear amplifier, the HSA can linearly and efficiently provide the supply voltage and current to the PA. The HSA itself operates optimally for the different PAPR signals. For the signal with a different bandwidth, the switching speed can be optimized by controlling the reference voltage of a comparator in the HSA. Thus, for the various standards with different signal BWs and PAPRs, the HSA can efficiently supply the DC power to the PA [12].

The overall efficiency of the ET transmitter is the multiplication of the efficiencies of the PA and the supply modulator.

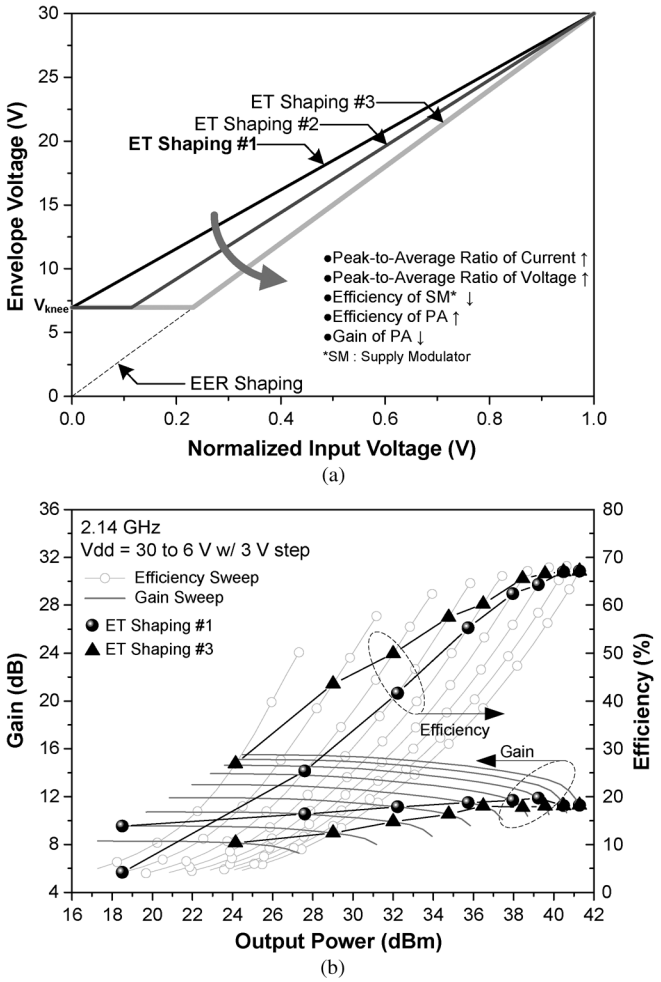

Fig. 17. (a) Various envelope shaping methods. (b) Measured gain and efficiency according to the supply voltage at 2.14 GHz. Additionally, estimated gain and efficiency for ET operation with the ET shaping #1 and #3 are overlaid.

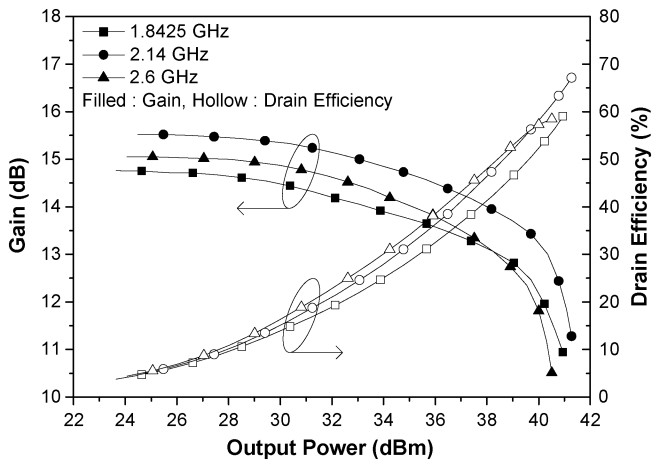

Fig. 18. Measured gain and efficiency performances at 1.8425, 2.14, and 2.6 GHz.

For the maximum efficiency and linear operation of the ET transmitter, the envelope shaping should be carefully considered because the efficiencies of the PA and the HSA are changed according to the envelope signal to be injected to the

TABLE II
MEASUREMENT SUMMARY OF ET PA

10-MHz BW 6.5-dB PAPR LTE Signal at 1.8425 GHz (ACLR1 at 7.50-MHz offset, ACLR2 at 12.50-MHz offset)						
	Output Power (dBm)	Gain (dB)	DE (%)	PAE (%)	ACLR1 (dBc)	ACLR2 (dBc)
Standalone PA w/o DPD	34.99	13.29	30.48	29.05	–25.14	–32.24
ET PA w/o DPD	35.00	10.83	35.75	32.79	–26.93	–33.07
ET PA w/ DPD	34.72	10.62	35.21	32.16	–45.20	–46.00
5-MHz BW 7.0-dB PAPR WCDMA Signal at 2.14 GHz (ACLR1 at 2.50-MHz offset, ACLR2 at 5.00-MHz offset)						
	Output Power (dBm)	Gain (dB)	DE (%)	PAE (%)	ACLR1 (dBc)	ACLR2 (dBc)
Standalone PA w/o DPD	35.00	14.18	34.34	33.02	–29.22	–38.00
ET PA w/o DPD	35.00	10.97	41.16	37.87	–28.74	–32.80
ET PA w/ DPD	34.73	10.60	40.79	37.24	–46.90	–47.50
10-MHz BW 8.5-dB PAPR m-WiMAX Signal at 2.6 GHz (ACLR1 at 5.32-MHz offset, ACLR2 at 6.05-MHz offset)						
	Output Power (dBm)	Gain (dB)	DE (%)	PAE (%)	ACLR1 (dBc)	ACLR2 (dBc)
Standalone PA w/o DPD	33.00	13.88	28.18	27.03	–26.80	–29.20
ET PA w/o DPD	33.01	9.31	31.57	27.87	–21.45	–24.55
ET PA w/ DPD	32.89	8.93	32.97	28.75	–44.30	–45.40

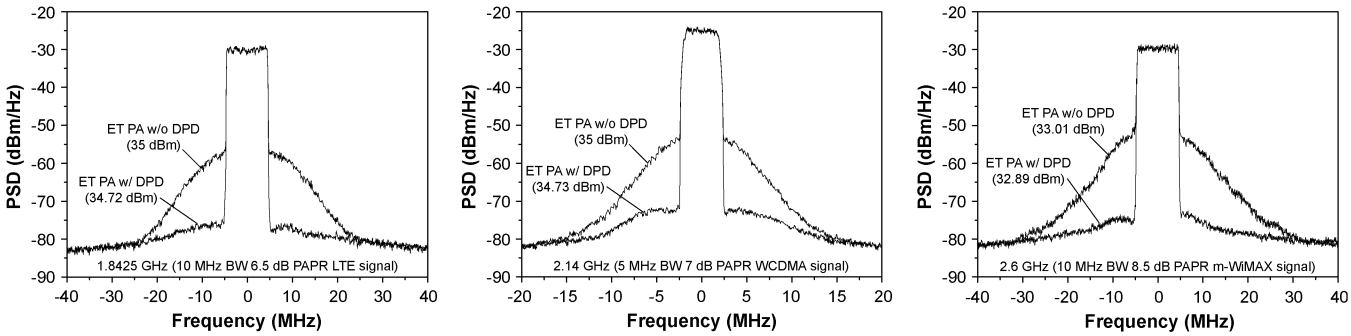

Fig. 19. Output spectras of the ET amplifiers at (a) 1.8425, (b) 2.14, and (c) 2.6 GHz before and after DPD.

PA. Moreover, the PA shows serious nonlinear characteristics at the supply voltage below the knee voltage $V_{\rm k}$ and the PA operation in the region should be avoided. Fig. 17(a) shows the various envelope shaping methods. To avoid the operation of the PA below $V_{\rm k}$, all shaping methods in Fig. 17(a) have an offset voltage. As the ET shaping approaches the EER shaping (Shaping #3) from ET Shaping #1, the PA in the ET transmitter operates in a deeply saturated region, degrading the linearity. Thus, as illustrated in Fig. 17(b), the efficiency of the PA is increased, but the gain is decreased. For the supply modulator, both peak-to-average ratios of the voltage and current to be amplified by HSA are increased so that the efficiency of the HSA is decreased. Therefore, in the interlock experiment, the envelope shaping function should be optimally selected considering the overall efficiency, gain, and linearity.

The multimode/multiband ET operations are demonstrated at the same frequency bands in Section II-D. For the LTE, WCDMA, and m-WiMAX signals, the implemented HSA delivers the efficiencies of 67.9, 67.5, and 60% with a constant load impedance of 50 Ω, which is the average load impedance seen into the drain bias port of the implemented broadband saturated amplifier. The lower efficiency for the m-WiMAX signal is caused by the higher PAPR. The envelope signal applied to the amplifier is shaped to maximize PAE performance. In particular, ET Shaping #1 in Fig. 17(a) is applied to modify the original envelope voltage, and $V_{\rm k}$ is set to 7 V. Fig. 18 shows the measured efficiency and gain characteristics for a CW signal at the three frequencies. The implemented amplifier provides the maximum efficiencies of 59.0, 67.1, and 58.5% for the frequencies at the saturated output power of 40.9, 41.3, and 40.5 dBm, respectively. Fig. 19 shows the measured output spectras of the ET amplifiers before and after linearization by the digital predistortion (DPD). The enhanced Hammerstein structure is employed to compensate for both static and dynamic nonlinearities of the ET PA [25]. The interlock experimental results are summarized in Table II. Since the ET amplifiers operate at the saturated region for all supply voltages, the gains are degraded. However, PAEs for LTE, WCDMA, and m-WiMAX applications are improved by 3.1, 4.2, and 1.7%, respectively, in comparison with the standalone PA. By adopting the DPD technique, the linearity performances are within the system requirements. The efficiency of the HSA is not the state-of-the-art and the ET efficiencies can be improved further using the HSA with higher efficiency.

IV. Conclusions

A multimode/multiband ET transmitter consisting of a HSA and a broadband saturated amplifier is presented. For the various wireless applications with different BW and PAPR, a highly efficient operation of HSA is accomplished by adapting the reference value of the hysteresis comparator. Since a saturated PA takes advantage of the nonlinear output capacitor to shape the voltage waveform, the PA maintains high efficiency operation across the wide bandwidth with the harmonic load higher than the output capacitor. This characteristic enables the saturated PA to operate with broadband characteristic and high efficiency because the design can be focused on the fundamental matching problem and the harmonic matching network has a large tolerance. The fundamental load and source impedances are found from the load/source-pull methodology. Then, the broadband matching networks are synthesized by SRFT. For the bandwidth from 1.3 to 2.7 GHz, the measured output power, DE, and PAE performances are between 39.8–42.0 dBm, 55.8–69.7%, and 51.2–65.3%, respectively. The ET transmitter is demonstrated at 1.8425-GHz LTE, 2.14-GHz WCDMA, and 2.6-GHz m-WiMAX applications. The transmitter delivers the PAE of 32.16, 37.24, and 28.75% for LTE, WCDMA, and m-WiMAX applications, respectively. By adopting the DPD technique, the linearity performances are within the system requirements.

Acknowledgment

The authors would like to thank Cree Inc., Durham, NC, for providing the GaN HEMT transistors and models used in this work.

References

[1] S. C. Cripps, *RF Power Amplifiers for Wireless Communications*, 2nd ed. Norwood, MA: Artech House, 2006.
[2] J. Choi, D. Kang, D. Kim, J. Park, B. Jin, and B. Kim, "Power amplifiers and transimitters for next generation mobile handset," *J. Semicond. Technol. Sci.*, vol. 9, no. 4, pp. 249–256, Dec. 2009.
[3] W. H. Doherty, "A new high efficiency power amplifier for modulated waves," *Proc. IRE*, vol. 24, no. 9, pp. 1163–1182, Sep. 1936.
[4] F. H. Raab, "Efficiency of Doherty RF power amplifier systems," *IEEE Trans. Broadcast.*, vol. BC-33, no. 3, pp. 77–83, Sep. 1987.
[5] Y. Yang, J. Yi, Y. Y. Woo, and B. Kim, "Optimum design for linearity and efficiency of microwave Doherty amplifier using a new load matching technique," *Microwave J.*, vol. 44, no. 12, pp. 20–36, Dec. 2001.
[6] J. Moon, J. Kim, J. Kim, and B. Kim, "Efficiency enhancement of Doherty amplifier through mitigation of the knee voltage effect," *IEEE Trans. Microw. Theory Tech.*, vol. 59, no. 1, pp. 143–152, Jan. 2011.
[7] D. Kang, D. Kim, J. Moon, and B. Kim, "Broadband HBT Doherty power amplifiers for handset applications," *IEEE Trans. Microw. Theory Tech.*, vol. 58, no. 12, pp. 4031–4039, Dec. 2010.
[8] K. Bathich, A. Z. Markos, and G. Boeck, "Frequency response analysis and bandwidth extension of the Doherty amplifier," *IEEE Trans. Microw. Theory Tech.*, vol. 59, no. 4, pp. 934–944, Apr. 2011.
[9] J. Moon, J. Kim, I. Kim, J. Kim, and B. Kim, "A wideband envelope tracking Doherty amplifier for WiMAX systems," *IEEE Microw. Wireless Compon. Lett.*, vol. 18, no. 1, pp. 49–51, Jan. 2008.
[10] L. Kahn, "Single-sideband transmission by envelope elimination and restoration," *Proc. IRE*, vol. 40, no. 7, pp. 803–806, Jul. 1952.
[11] B. Kim, J. Moon, and I. Kim, "Efficiently amplified," *IEEE Microw. Mag.*, vol. 11, no. 5, pp. 89–100, Aug. 2010.
[12] J. Choi, D. Kim, D. Kang, and B. Kim, "A polar transmitter with CMOS programmable hysteretic-controlled hybrid switching supply modulator for multi-standard applications," *IEEE Trans. Microw. Theory Tech.*, vol. 57, no. 7, pp. 1675–1686, Jul. 2009.
[13] D. F. Kimball, J. Jeong, C. Hsia, P. Draxler, S. Lanfranco, W. Nagy, K. Linthicum, L. E. Larson, and P. M. Asbeck, "High-efficiency envelope-tracking W-CDMA base-station amplifier using GaN HFETs," *IEEE Trans. Microw. Theory Tech.*, vol. 54, no. 11, pp. 3848–3856, Nov. 2006.
[14] D. Kang, D. Kim, J. Choi, J. Kim, Y. Cho, and B. Kim, "A multimode/multiband power amplifier with a boosted supply modulator," *IEEE Trans. Microw. Theory Tech.*, vol. 58, no. 10, pp. 2598–2608, Oct. 2010.
[15] P. Wright, J. Lees, J. Benedikt, P. J. Tasker, and S. C. Cripps, "A methodology for realizing high efficiency Class-J in a linear and broadband PA," *IEEE Trans. Microw. Theory Tech.*, vol. 57, no. 12, pp. 3196–3204, Dec. 2009.
[16] D. Y.-T. Wu, F. Mkadem, and S. Boumaiza, "Design of a broadband and highly efficient 45 W GaN power amplifier via simplified real frequency technique," in *IEEE MTT-S Int. Microw. Symp. Dig.*, Jun. 2010, pp. 1090–1093.
[17] P. Saad, C. Fager, H. Cao, H. Zirath, and K. Andersson, "Design of a highly efficient 2–4-GHz octave bandwidth GaN-HEMT power amplifier," *IEEE Trans. Microw. Theory Tech.*, vol. 58, no. 7, pp. 1677–1685, Jul. 2010.
[18] A. A. Tanany, D. Gruner, A. Sayed, and G. Boeck, "Highly efficient harmonically tuned broadband GaN power amplifier," in *Proc. 40th Eur. Microw. Conf.*, Sep. 2010, pp. 5–8.
[19] J. Moon, J. Son, J. Lee, J. Kim, S. Jee, S. Kim, and B. Kim, "A multimode/multiband envelope tracking transmitter with broadband saturated power amplifier," in *IEEE MTT-S Int. Microw. Symp. Dig.*, Jun. 2011, pp. 1–4.
[20] B. Kim, J. Moon, and J. Kim, "Highly efficient saturated power amplifier based on GaN—A class P amplifier," in *IEEE MTT-S Int. Microw. Symp. Dig. Workshop*, Anaheim, CA, May 2010, invited talk.
[21] J. Moon, J. Kim, and B. Kim, "Investigation of a class-J power amplifier with a nonlinear $C_{\rm out}$ for optimized operation," *IEEE Trans. Microw. Theory Tech.*, vol. 58, no. 11, pp. 2800–2811, Nov. 2010.
[22] J. Kim, J. Kim, J. Moon, J. Son, I. Kim, S. Jee, and B. Kim, "Saturated power amplifier optimized for efficiency using self-generated harmonic current and voltage," *IEEE Trans. Microw. Theory Tech.*, vol. 59, no. 8, pp. 2049–2058, Aug. 2011.
[23] B. S. Yarman and H. Carlin, "A simplified real frequency technique applied to broad-band multistage microwave amplifiers," *IEEE Trans. Microw. Theory Tech.*, vol. 30, no. 12, pp. 2216–2222, Dec. 1982.
[24] B. S. Yarman, *Design of Ultra Wideband Antenna Matching Networks*. New York: Springer Netherlands, 2008.
[25] J. Moon and B. Kim, "Enhanced Hammerstein behavioral model for broadband wireless transmitters," *IEEE Trans. Microw. Theory Tech.*, vol. 59, no. 4, pp. 924–933, Apr. 2011.

Junghwan Moon (S'07) received the B.S. degree in electrical and computer engineering from the University of Seoul, Seoul, Korea, in 2006 and is currently working toward the Ph.D. degree at the Pohang University of Science and Technology (POSTECH), Pohang, Gyeongbuk, Korea.

His current research interests include highly linear and efficient RF PA design, memory-effect compensation techniques, digital predistortion (DPD) techniques, and wideband RF PA design.

Mr. Moon was the recipient of the Highest Efficiency Award at Student High-Efficiency Power Amplifier Design Competition in IEEE MTT-S International Microwave Symposium (IMS), 2008 and the First Place Award at Student High-Efficiency Power Amplifier Design Competition in IEEE MTT-S IMS, 2011.

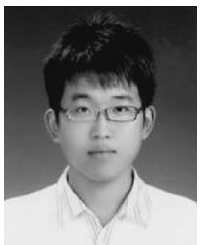

Junghwan Son received the B.S. degree in physics from Sejong University, Seoul, Korea, in 2008, and the M.S. degree in computer and communications engineering in from the Pohang University of Science and Technology (POSTECH), Pohang, Gyeongbuk, Korea, in 2010, and currently working toward the Ph.D. degree in electrical and electronics engineering at the POSTECH.

His current research interests include RF PA design and linearity enhancement technique.

Juyeon Lee received the B.S. degree in electrical engineering from the Pohang University of Science and Technology (POSTECH), Pohang, Korea, in 2011, and is currently working toward the Ph.D. degree in electrical engineering from POSTECH.

His current research interests include highly efficient RF power amplifier design.

Mr. Lee was the recipient of the First Place Award at Student High-Efficiency Power Amplifier Design Competition in IEEE MTT-S International Microwave Symposium (IMS), 2011.

Bumman Kim (M'78–SM'97–F'07) received the Ph.D. degree in electrical engineering from Carnegie Mellon University, Pittsburgh, PA, in 1979.

From 1978 to 1981, he was engaged in fiber-optic network component research with GTE Laboratories Inc. In 1981, he joined the Central Research Laboratories, Texas Instruments Incorporated, where he was involved in development of GaAs power field-effect transistors (FETs) and monolithic microwave integrated circuits (MMICs). He has developed a large-signal model of a power FET, dual-gate FETs for gain control, high-power distributed amplifiers, and various millimeter-wave MMICs. In 1989, he joined the Pohang University of Science and Technology (POSTECH), Pohang, Gyeongbuk, Korea, where he is a POSTECH Fellow and a Namko Professor with the Department of Electrical Engineering, and Director of the Microwave Application Research Center, where he is involved in device and circuit technology for RF integrated circuits (RFICs). He has authored over 300 technical papers.

Prof. Kim is a member of the Korean Academy of Science and Technology and the National Academy of Engineering of Korea. He was an associate editor for the IEEE TRANSACTIONS ON MICROWAVE THEORY AND TECHNIQUES, a Distinguished Lecturer of the IEEE Microwave Theory and Techniques Society (IEEE MTT-S), and an AdCom member.